# Ultrafast Transition from State-Blocking Dynamics to Electron Localization in Transition Metal $\beta$-Tungsten

E. W. de Vos, * S. Neb, A. Niedermayr, F. Burri, M. Hollm, L. Gallmann, and U. Keller
*Department of Physics, ETH Zürich, 8093 Zürich, Switzerland*

(Received 10 March 2023; revised 27 August 2023; accepted 17 October 2023; published 27 November 2023)

We describe an ultrafast transition of the electronic response of optically excited transition metal $\beta$-tungsten with few-femtosecond time resolution. The response moves from a regime where state filling of the excited carrier population around the Fermi level dominates towards localization of carriers onto the outer $d$ orbitals. This is in contrast to previous measurements using ultrafast element-specific core-level spectroscopy enabled by attosecond transient absorption spectroscopy on transition metals such as titanium and around the transition metal atom in transition metal dichalchogenides $MoTe_2$ and $MoSe_2$. This surprisingly different dynamical response for $\beta$-tungsten can be explained by considering the electron-electron dynamics on a few-femtosecond timescale and the slower electron-phonon thermalization dynamics.

DOI: 10.1103/PhysRevLett.131.226901

The understanding of electron dynamics on ultrafast timescales is needed in order to push electronics towards the THz and even PHz frequencies. Of particular significance are materials containing transition metal elements, given their potential integration into high-frequency optoelectronic devices. Recently, ultrafast electron localization into $d$ orbitals surrounding a transition metal element has been directly observed to occur within less than a few femtoseconds in metals [1] and semiconductors [2]. This observation challenges the adequacy of the independent electron approximation. Therefore, a fundamental question remains unanswered: when can we accurately describe an optically excited solid using the free-electron approximation with the very successful effective mass approximation, and when do collective electron phenomena predominate in its response? This question persists due to the varying strengths of numerous dynamical interactions during and after excitation, such as Pauli state blocking [3–5], the dynamical Franz Keldysh effect [6–10], and electron localization [1,11–13] as well as the relaxation of excited electrons due to coupling to plasmons [14–16], phonons [12,17–21], and other electrons [22–26]. In this study, we demonstrate that in the response of the transition metal $\beta$-tungsten both independent and collective electron phenomena play an important role. The initial response is surprisingly governed by free-electron dynamics, however, this later transitions into the more typical collective response, previously observed for transition metal elements.

Attosecond transient absorption spectroscopy (ATAS) is a pump-probe spectroscopic technique ideally suited for investigating both the optical excitation of electrons and their subsequent relaxation [27,28]. In ATAS experiments on solids the electron dynamics in thin-film samples are typically driven by few-cycle near-infrared (NIR) to mid-infrared (MIR) pulses and probed via the absorption of broadband XUV single attosecond pulses (SAPs) or attosecond pulse trains (APTs). The temporal profile of these pulses naturally allows for sub-femtosecond resolution of the induced dynamics. Broadband XUV spectroscopy additionally allows for simultaneous probing of both occupied and unoccupied states around the Fermi level in metals or both the valence and the conduction band in semiconductors from multiple core states, enabling the observation of element specific dynamics.

Prior ATAS investigations of solids have yielded significant insights. An examination of the simple metal aluminum revealed that the pump-induced change in absorption could be accurately reproduced by an independent particle model, which exclusively considers state blocking [4]. When we only consider state blocking, the decrease in absorption of the XUV probe is purely governed by the blocking of probe transitions by the excited state population above the Fermi energy ($E_F$) and the increase in absorption through the depletion of electrons below $E_F$.

In contrast, investigations into the transition metal titanium required TDDFT simulations that included the induced, ultrafast localization of the excited electron population onto its valence $3d$ orbitals for good agreement with the measurements [1]. This localization, characterized

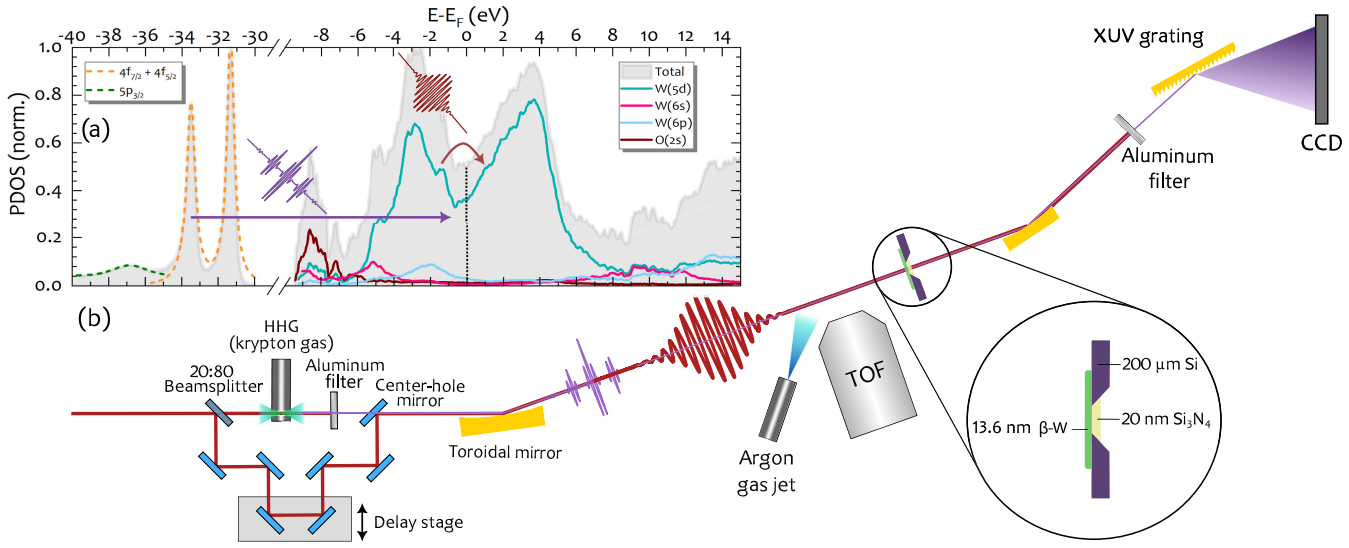


FIG. 1. (a) Electronic density of states (DOS) of $\beta$-tungsten. The relevant core states between −40 and −30 eV are depicted on the left, and are based on data obtained in Ref. [37] (solid gray), fitted with Lorentzian peaks (dashed lines) and normalized to the $4f_{7/2}$ resonance. On the right, the angular momentum projected density of states (PDOS) around the Fermi energy $E_F$ of $\beta$-tungsten with a 15.79% atomic percentage of oxygen is shown. The PDOS is dominated by $5d$ orbitals and contributions from the oxygen atoms are negligible. PDOS data around $E_F$ is taken from an extended calculation of Ref. [33]. (b) Sketch of the high harmonic generation (HHG) and measurement section of the attosecond transient absorption spectroscopy (ATAS) setup. Both the front section (beam splitter–toroidal mirror, $10^{-4}$–$10^{-6}$ mbar) and the measurement section (TOF–CCD, $10^{-7}$–$10^{-9}$ mbar) are kept at high vacuum.

by $d$-orbital-shaped changes in electron density around the Ti atom, in turn, screened the inner core orbitals, effectively compensating for the state-blocking effect. The relatively large dynamical response of titanium followed the pulse fluence of a few femtoseconds and can therefore be assumed to occur on an even shorter timescale. Both regimes of ultrafast localization and state blocking have been found to occur simultaneously but separately for the two atomic constituents of the transition metal dichalcogenides (TMDCs) $MoTe_2$ [29] and $MoSe_2$ [2]. In these semiconductor materials, the element-specific ATAS signal around the transition metal molybdenum was predominantly governed by the same dynamics of ultrafast localization-induced screening observed in titanium, while the signal around the chalcogens resulted from band filling, also known as state blocking.

In our study of the transition metal $\beta$-tungsten we observe an ultrafast transition from a regime where state blocking of the excited electron distribution around the Fermi energy dominates, towards a regime where the screening induced by localization of the excited population onto the outer $d$ orbitals of $\beta$-tungsten is dominant. Additionally, in contrast to titanium, the initial response of $\beta$-tungsten does not follow the pump's integrated photon flux, instead exhibiting temporal broadening due to electron-electron thermalization.

The transition metal $\beta$-tungsten is an allotrope of tungsten which, instead of the usual bcc crystallographic structure ($\alpha$-tungsten), exhibits an A15 cubic phase [30–33]. This is a metastable phase of tungsten that is stabilized by oxygen defects and only occurs in films with a thickness below a critical value, which depends on growth conditions and can reach up to 60 nm [34]. $\beta$-tungsten exhibits many interesting electronic properties, such as an increased superconducting temperature as compared to $\alpha$-tungsten [35], and has recently seen a revival in scientific interest due to the finding of a giant spin Hall effect [34,36]. For the purpose of the experiment described in this Letter, it is important to note that it is a transition metal with unfilled $5d$ orbitals and that we can probe the dynamics around the Fermi level via core transitions from both a spin-orbit split $4f$ initial state as well as a $5p$ core state [see Fig. 1(a)].

The pump-probe ATAS setup that was used is described in detail in Ref. [38] and is schematically shown in Fig. 1(b). 80% of a ∼300 μJ NIR pulse with a center photon energy of 1.68 eV is focused into a krypton gas jet and produces an APT with a spectrum ranging from 27 to 46 eV [see Fig 3(a)]. A 100-nm thin-film of aluminum filters out the residual NIR beam and the XUV probe is then recombined with the temporally delayed NIR pump beam via a center-hole mirror. An iris in the pump arm of the setup is used to adjust the pulse energy of the pump pulse. For the measurements depicted in this Letter, a pulse energy of 0.7 μJ at a repetition rate of 1 kHz was used. A gold toroidal mirror at grazing incidence focuses both beams onto the target and a time of flight (TOF) setup is used to characterize the pump pulse *in situ* after the measurement and to calibrate the pump-probe delay via reconstruction of attosecond beating by interference of two-photon transitions (RABBITT) [39]. The sample consists of a 13.6-nm

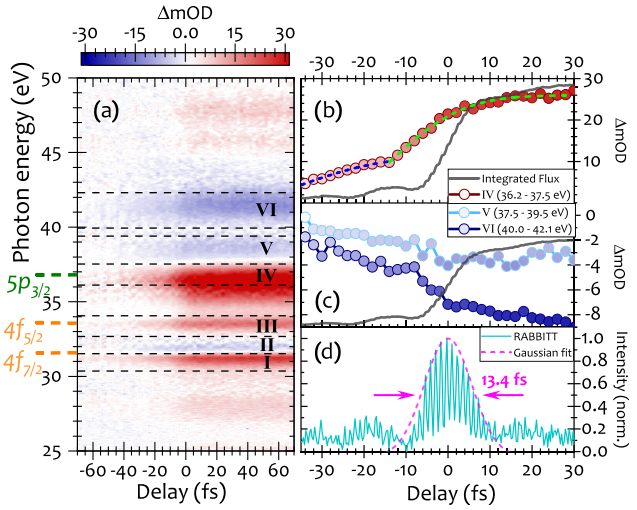


FIG. 2. (a) ATAS measurement of the few-femtosecond dynamics around pump-probe overlap of the rise of the pump-induced changes in milli-optical density ($\Delta\text{mOD} = 10^{-3}\Delta\text{OD}$) for thin-film $\beta$-tungsten. Induced opacity is depicted in red and induced transparency in blue. Different energy intervals are labeled with Roman numerals. Zero time delay was calibrated by the peak of the RABBITT sideband trace, depicted in panel (d), which represents the cross correlation between the NIR pulse and the APT. (b),(c) Averaged temporal profile of changes in optical density during pump-probe overlap, for specific features (red and blue circles). The integrated photon flux of the *in situ* RABBITT measurement is depicted in gray. (d) RABBITT characterization of the NIR pump pulse (sideband 22) with Gaussian envelope fits (dashed pink). The main pulse has a temporal FWHM of 13.4 fs and a small pre-pulse centered at −19.2 fs is also present.

layer of $\beta$-W that was deposited onto a 20-nm $Si_3N_4$ substrate using electron beam evaporation. The presence of $\beta$-W was confirmed with transmission x-ray diffraction, performed after the ATAS measurements.

The change in optical density is defined as

$$\Delta\text{OD}(E,t) = \ln\left(\frac{I_{\text{XUV}}}{I_{\text{XUV+NIR}}(t)}\right), \tag{1}$$

where $I_{\text{XUV}}$ and $I_{\text{XUV+NIR}}$ represent the spectral intensity distributions of the XUV probe that are transmitted through the sample with the shutter in the pump arm closed and open, respectively.

Figure 2(a) depicts the results of an ATAS measurement of the initial rise of the change in optical density (ΔOD) after excitation by the NIR pump pulse. The derivative ΔOD features from negative to positive ΔOD at 31.8 (region I and II) and 37.5 eV (region IV and V) are characteristic of NIR-induced state-blocking as probed by the XUV probe from the $4f_{7/2}$ and $5p_{3/2}$ core orbitals, respectively [3,5]. Furthermore, the spectral widths of these features (0.61 and 1.73 eV, respectively) approximately match the spectral widths of the core states (0.33 and 1.85 eV, respectively), extracted from Gaussian fits to hard x-ray photoelectron spectroscopy data from Ref. [40]. A similar derivative feature is expected for the probing from the $4f_{5/2}$ orbital (region III), with a binding energy of 33.6 eV; however, its induced transparency is most likely obscured by the energetically broad response in region IV from the $5p$ probing. Additionally, a broad negative ΔOD feature is observed between 40 and 43 eV (region VI). This feature is likely due to an oxidation layer on the $\beta$-$W/Si_3N_4$ interface and is discussed in detail in the Supplemental Material [41].

Figures 2(b) and 2(c) depict the average induced ΔOD throughout excitation for selected spectral regions, compared to the integrated photon flux of the NIR pulse. For both the positive feature in Fig. 2(b) and the negative features in Fig. 2(c) a two-step rise is observed. The signal starts at a slight increase in NIR pump flux—corresponding to a small pre-pulse—for delays as low as −30 fs compared to temporal center of the pump pulse (see Fig. 2(d), which depicts a Gaussian fit of a lineout of sideband 22 of an *in situ* RABBITT measurement of the NIR pump pulse). Once the main pulse arrives, the rise of these features becomes steeper and flattens off after pump-probe overlap. The dashed blue and green lines in Fig. 2(b) depict two separate Gaussian error function fits for each of the two-step rise.

Rather than directly following the pump flux, the rise of the ΔOD features during excitation is smeared out over a longer temporal range. A similar flux-dependent effect was observed and simulated for the transition metal nickel [48] and related to nonthermal electron-electron relaxation. Typical electron-electron thermalization times of laser-excited metals under similar experimental conditions range from the few-fs regime up to several tens of femtoseconds [26,48] and depend on the induced final electron temperature. Fitting the two-step rise of the feature in region IV with two Gaussian error functions, we get a rise time ($\tau_{\text{rise}}$) associated with the main pulse of $32.9 \pm 6.0$ fs. This is larger than the cross-correlation time of the pump pulse with the probe pulse train, $t_{\text{cc}} = 13.4 \pm 0.9$ fs, that can be extracted from the envelope fit of the RABBITT sideband. A detailed description of the fitting procedure for the ΔOD-features can be found in the Supplemental Material [41]. As in Ref. [48] we can deconvolve these timescales to obtain a thermalization time of $\tau_{\text{e-e}} \approx \sqrt{\tau_{\text{rise}}^2 - t_{\text{cc}}^2} = 30.0 \pm 6.6$ fs. This value fits appropriately within previously reported thermalization times for optically excited metals [26].

Using Fermi liquid theory, we can now relate the electron-electron thermalization time to the final electron temperature $T_e$ [20,49]:

$$T_e \approx \frac{1}{k_b \mu_c}\sqrt{\frac{4\hbar E_F}{\pi^3 \tau_{\text{e-e}}}} \approx 2700\ \text{K}, \tag{2}$$

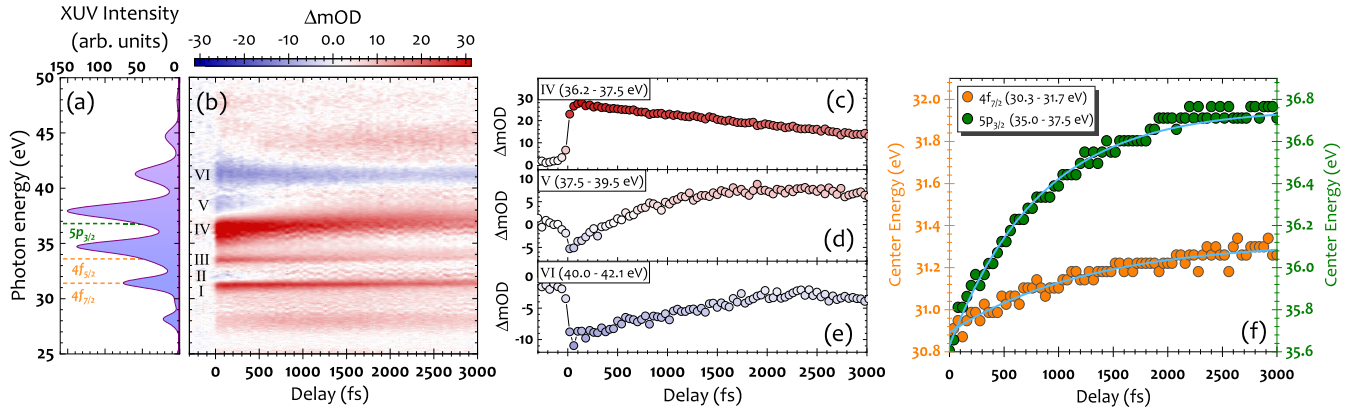


FIG. 3. (a) High harmonic XUV probe spectrum, ranging from approximately 27 to 46 eV, generated in krypton. (b) Transient absorption spectrogram of the few-picosecond dynamics after pump-probe overlap. Induced opacity is depicted in red and induced transparency in blue. (c),(d),(e) Averaged temporal profile of changes in optical density for specific probe energy ranges. (f) Temporal evolution of the center of energy along the spectral axis of the positive features between 30.3 and 31.7 eV (orange) and 35.0 and 37.5 eV (green), which result from probing the $4f_{7/2}$ and $5p_{3/2}$ initial states, respectively. Spectral shifts of 0.2 and 0.45 eV are observed.

with $\mu_c = r_s/2\pi$ the Coulomb pseudopotential, where $r_s = 3.3$ is the ratio between the Wigner-Seitz radius and the Bohr radius [50]. The values for $r_s$ and $E_F = 5.78$ eV [51] are taken for tungsten rather than $\beta$-tungsten because of their availability in literature.

On the few-picosecond timescale [see Fig. 3] we can observe electron-phonon thermalization. This is most notable in the positive ΔOD-feature that is present between 35.0 and 37.5 eV and can also be observed for the positive feature between 30.3 and 31.8 eV. Both of these features narrow within the first few picoseconds, which corresponds to a cooling of the excited Fermi-Dirac distribution. From the temporal evolution of the center of energy along the spectral axis for both features [see Fig. 3(f)], we see that they shift upward by 0.2 and 0.45 eV within a characteristic timescale ($\tau_{\text{e-ph}}$) of $1.3 \pm 0.1$ ps. Here, $\tau_{\text{e-ph}}$ is defined as the time constant of a sigmoidal logistic fit (solid blue lines).

On the same timescales as the electron-phonon relaxation, we can observe a diminishing of the negative ΔOD-features in regions II and V. Directly after excitation, these features and their adjacent positive signals at lower energies resemble a response that is typical for state blocking. In this context, the NIR pump causes energetic broadening of the Fermi-Dirac distribution and reduces the number of available states for the XUV probe above $E_F$, leading to an induced transparency, and increases the number of available states below $E_F$, leading to an induced opacity. The center energy of the gap between the positive and negative features resembles the separation between the energy of the probing core hole and $E_F$ and is 31.6 eV for the lower feature and 37.5 eV for the upper feature. This compares well with the theoretical values of 31.3 and 37.2 eV for the $4f_{7/2}$ and the $5p_{3/2}$ states, respectively [52].

However, contrary to the other features of the spectrogram, the induced transparent signal above $E_F$ disappears after approximately 500 fs for the probing from the $4f_{7/2}$ and the $5p_{3/2}$ state. These signals continue to rise, eventually resulting in a positive ΔOD-signal that peaks after 2 ps. This means that after electron-phonon thermalization, the resulting spectrogram between 27 and 40 eV is purely positive. This positive signal is exactly what was observed for transition metal Ti [1] and around the transition metal atom Mo in the TMDC semiconductor materials $MoSe_2$ and $MoTe_2$ [2,29]. For Ti and Mo, TDDFT calculations showed that the excited carriers localize onto the outer $d$ orbitals, which in turn induces a screening of the core states. This screening effect was found to cancel out the effect of state blocking and therefore reduced the typical positive-to-negative derivative structure to a purely positive signal. This was not observed for Al [4] and around the chalchogenide atoms Te and Se in $MoTe_2$ [29] and $MoSe_2$ [2].

Similar to titanium, $\beta$-tungsten has an unfilled outer $d$-orbital shell onto which the excited carriers can localize. However, in the case of $\beta$-tungsten, we can now observe an ultrafast transition from an initial regime ($0 < t < 500$ fs after excitation) where state blocking dominates towards a regime ($t > 500$ fs) where screening dominates. Because of the similar timescales involved, we assume that the electron-phonon thermalization effectively reduces the signal contribution of the state blocking that is a consequence of the excited population dynamics. The localization of the excited population onto the outer $d$ orbitals, however, persists for a larger timescale. The signal thus moves from a state where it is initially dominated by an independent particle response towards a regime where we need to account for collective electron dynamics. It is also important to note that the signal for $t > 500$ fs is most likely not purely thermal in nature, as this would induce an increase of the electron population above $E_F$ and therefore cause a negative ΔOD signal.

To address the difference in the response between titanium and $\beta$-tungsten, we consider the difference in electronic density of states between these two materials. Although for both titanium and $\beta$-tungsten the DOS is dominated by $d$ orbitals around $E_F$, there are two significant differences. First of all, in titanium $3d$ orbitals are responsible for the screening response, whereas for $\beta$-tungsten we excite $5d$ orbitals. As $5d$ states are more delocalized as compared to $3d$ states, we expect the localization of excited electrons onto $5d$ orbitals to lead to a less efficient screening.

More importantly, however, for $\beta$-tungsten the Fermi energy lies in a "pseudo-gap" of the DOS, with the distribution of $5d$ states peaking at approximately 3 eV below and 3.5 eV above $E_F$. In titanium, however, the DOS peaks almost immediately above $E_F$. We can now use the final electron temperature $T_e$, which we extracted from the electron-electron thermalization time, to approximate the excited electronic states with a Fermi-Dirac distribution for $\beta$-tungsten. A convolution of the excited Fermi-Dirac distribution of $\beta$-tungsten and titanium with their $d$-orbital DOS shows that in the study on titanium approximately 4 times more $d$ states were excited compared to $\beta$-tungsten (details in the Supplemental Material [41]). This explains why the screening response is able to initially fully cancel out the state-blocking population dynamics in titanium, whereas for $\beta$-tungsten this can only happen after the excited population has significantly thermalized through interaction with the lattice.

In conclusion, we provide a direct, time-resolved perspective on the emergence of collective electron behavior within a transition metal. We have observed an ultrafast transition within $\beta$-tungsten, spanning from a regime where state blocking and the pump-induced broadening of the Fermi-Dirac distribution predominate to a regime where electron localization and induced screening take precedence. Notably, this stands in contrast to previous measurements involving other transition metal atoms like Ti [1] and Mo in TMDCs [2]. We have quantified this transition by examining electron-electron and electron-phonon thermalization dynamics across distinct timescales, ranging from a few femtoseconds to picoseconds. The observation that free-electron dynamics can govern the initial response of optically excited transition metals, but then transitions into a collective response, bears significant implications for comprehending their signal rise times and their incorporation in ultrafast electronics.

The authors kindly acknowledge A. Kanjilal, V. Kumar, and A. Chattaraj for extending the calculation from Ref. [33] of the PDOS for $\beta$-tungsten, which was adapted into Fig. 1(a). This research was supported by the Swiss National Science Foundation (SNSF) Project No. 200020-200416. S. N. is supported by funding from European Union's Horizon 2020 under Marie Skłodowska-Curie COFUND Action Grant No. 801459, FP-RESOMUS.

*edevos@phys.ethz.ch

[1] M. Volkov, S. A. Sato, F. Schlaepfer, L. Kasmi, N. Hartmann, M. Lucchini, L. Gallmann, A. Rubio, and U. Keller, Nat. Phys. **15**, 1145 (2019).
[2] Z. Schumacher, S. A. Sato, S. Neb, A. Niedermayr, L. Gallmann, A. Rubio, and U. Keller, arXiv:2210.05465.
[3] M. Zürch, H. T. Chang, L. J. Borja, P. M. Kraus, S. K. Cushing, A. Gandman, C. J. Kaplan, M. H. Oh, J. S. Prell, D. Prendergast, C. D. Pemmaraju, D. M. Neumark, and S. R. Leone, Nat. Commun. **8**, 15734 (2017).
[4] A. Niedermayr, M. Volkov, S. A. Sato, N. Hartmann, Z. Schumacher, S. Neb, A. Rubio, L. Gallmann, and U. Keller, Phys. Rev. X **12**, 021045 (2022).
[5] F. Schlaepfer, M. Lucchini, S. A. Sato, M. Volkov, L. Kasmi, N. Hartmann, A. Rubio, L. Gallmann, and U. Keller, Nat. Phys. **14**, 560 (2018).
[6] A. P. Jauho and K. Johnsen, Phys. Rev. Lett. **76**, 4576 (1996).
[7] M. Lucchini, S. A. Sato, A. Ludwig, J. Herrmann, M. Volkov, L. Kasmi, Y. Shinohara, K. Yabana, L. Gallmann, and U. Keller, Science **353**, 916 (2016).
[8] A. Picón, L. Plaja, and J. Biegert, New J. Phys. **21**, 043029 (2019).
[9] L. Keldysh, J. Exp. Theor. Phys. **33**, 994 (1958), http://jetp.ras.ru/cgi-bin/e/index/e/6/4/p763?a=list.
[10] W. Franz, Z. Naturforsch. Teil A **13**, 484 (1958).
[11] E. E. Krasovskii and W. Schattke, Phys. Rev. B **60**, R16251 (1999).
[12] M. Bauer, A. Marienfeld, and M. Aeschlimann, Prog. Surf. Sci. **90**, 319 (2015).
[13] S. Neppl, R. Ernstorfer, A. L. Cavalieri, C. Lemell, G. Wachter, E. Magerl, E. M. Bothschafter, M. Jobst, M. Hofstetter, U. Kleineberg, J. V. Barth, D. Menzel, J. Burgdörfer, P. Feulner, F. Krausz, and R. Kienberger, Nature (London) **517**, 342 (2015).
[14] S. Xu, C. C. Miller, J. Cao, D. A. Mantell, M. G. Mason, A. A. Muenter, B. A. Parkinson, R. J. D. Miller, and Y. Gao, J. Vac. Sci. Technol. **15**, 1510 (1997).
[15] G. F. Giuliani and J. J. Quinn, Phys. Rev. B **26**, 4421 (1982).
[16] P. Hawrylak, G. Eliasson, and J. J. Quinn, Phys. Rev. B **37**, 10187 (1988).
[17] D. Mongin, P. Maioli, J. Burgin, P. Langot, E. Cottancin, S. D'Addato, B. Canut, M. Treguer, A. Crut, F. Vallee, and N. D. Fatti, J. Phys. Condens. Matter **31**, 084001 (2019).
[18] E. Bevillon, J. P. Colombier, V. Recoules, and R. Stoian, Phys. Rev. B **89**, 115117 (2014).
[19] G. Du, Q. Yang, F. Chen, Y. Wu, Y. Ou, Y. Lu, and X. Hou, Int. J. Heat Mass Transfer **87**, 341 (2015).
[20] C. Gadermaier, A. S. Alexandrov, V. V. Kabanov, P. Kusar, T. Mertelj, X. Yao, C. Manzoni, D. Brida, G. Cerullo, and D. Mihailovic, Phys. Rev. Lett. **105**, 257001 (2010).
[21] Z. Lin, L. V. Zhigilei, and V. Celli, Phys. Rev. B **77**, 075133 (2008).
[22] N. Del Fatti, C. Voisin, M. Achermann, S. Tzortzakis, D. Christofilos, and F. Vallee, Phys. Rev. B **61**, 16956 (2000).
[23] J. Garduño-Mejía, M. P. Higlett, and S. R. Meech, Surf. Sci. **602**, 3125 (2008).
[24] V. V. Kabanov, Low Temp. Phys. **46**, 414 (2020).

[25] M. v. Kampen, J. T. Kohlhepp, W. J. M. d. Jonge, B. Koopmans, and R. Coehoorn, J. Phys. Condens. Matter **17**, 6823 (2005).
[26] B. Y. Mueller and B. Rethfeld, Phys. Rev. B **87**, 035139 (2013).
[27] A. Zong, B. R. Nebgen, S.-C. Lin, J. A. Spies, and M. Zuerch, Nat. Rev. Mater. **8**, 224 (2023).
[28] R. Geneaux, H. J. B. Marroux, A. Guggenmos, D. M. Neumark, and S. R. Leone, Phil. Trans. R. Soc. A **377**, 20170463 (2019).
[29] A. R. Attar, H. T. Chang, A. Britz, X. Zhang, M. F. Lin, A. Krishnamoorthy, T. Linker, D. Fritz, D. M. Neumark, R. K. Kalia, A. Nakano, P. Ajayan, P. Vashishta, U. Bergmann, and S. R. Leone, ACS Nano **14**, 15829 (2020).
[30] H. Hartmann, F. Ebert, and O. Bretschneider, Z. Anorg. Allg. Chem. **198**, 116 (1931).
[31] A. B. Kiss, J. Therm. Anal. Calorim. **54**, 815 (1998).
[32] A. Chattaraj, M. Balal, A. K. Yadav, S. R. Barman, A. K. Sinha, S. N. Jha, S. Joulie, V. Serin, A. Claverie, V. Kumar, and A. Kanjilal, Sci. Rep. **10**, 14718 (2020).
[33] A. Chattaraj, S. Joulie, V. Serin, A. Claverie, V. Kumar, and A. Kanjilal, Sci. Rep. **12**, 3865 (2022).
[34] R. Bansal, G. Nirala, A. Kumar, S. Chaudhary, and P. K. Muduli, SPIN **08**, 1850018 (2018).
[35] S. Basavaiah and S. R. Pollack, J. Appl. Phys. **39**, 5548 (1968).
[36] M. Costa, A. T. Costa, J. Hu, R. Q. Wu, and R. B. Muniz, J. Phys. Condens. Matter **30**, 305802 (2018).
[37] D. Mueller, A. Shih, E. Roman, T. Madey, R. Kurtz, and R. Stockbauer, J. Vac. Sci. Technol. **6**, 1067 (1988).
[38] R. Locher, M. Lucchini, J. Herrmann, M. Sabbar, M. Weger, A. Ludwig, L. Castiglioni, M. Greif, M. Hengsberger, L. Gallmann, and U. Keller, Rev. Sci. Instrum. **85**, 013113 (2014).
[39] H. Muller, Appl. Phys. B **74**, s17 (2002).
[40] C. Kalha, L. E. Ratcliff, J. J. G. Moreno, S. Mohr, M. Mantsinen, N. K. Fernando, P. K. Thakur, T.-L. Lee, H.-H. Tseng, T. S. Nunney, J. M. Kahk, J. Lischner, and A. Regoutz, Phys. Rev. B **105**, 045129 (2022).
[41] See Supplemental Material at http://link.aps.org/supplemental/10.1103/PhysRevLett.131.226901 for a discussion of the fitting procedure for the electron thermalization time, the estimation of the excited DOS population and a discussion of observed acoustical phonons, which includes Refs. [42–47].
[42] V. A. Semenov, O. A. Dubovsky, A. V. Orlov, D. V. Savostin, and V. V. Sudarev, Phys. Solid State **56**, 29 (2014).
[43] H. Park, X. Wang, S. Nie, R. Clinite, and J. Cao, Phys. Rev. B **72**, 100301(R) (2005).
[44] J. Chen, W.-K. Chen, J. Tang, and P. M. Rentzepis, Proc. Natl. Acad. Sci. U.S.A. **108**, 18887 (2011).
[45] S. K. Cushing, M. Zürch, P. M. Kraus, L. M. Carneiro, A. Lee, H.-T. Chang, C. J. Kaplan, and S. R. Leone, Struct. Dyn. **5**, 054302 (2018).
[46] O. A. Lukianova and V. V. Sirota, Ceram. Int. **43**, 8284 (2017).
[47] A. Nagakubo, H. T. Lee, H. Ogi, T. Moriyama, and T. Ono, Appl. Phys. Lett. **116**, 021901 (2020).
[48] H.-T. Chang, A. Guggenmos, S. K. Cushing, Y. Cui, N. U. Din, S. R. Acharya, I. J. Porter, U. Kleineberg, V. Turkowski, T. S. Rahman, D. M. Neumark, and S. R. Leone, Phys. Rev. B **103**, 064305 (2021).
[49] N. W. Ashcroft and Mermin, *Solid State Physics*, 35th ed. (Brooks/Cole, South Melbourne, 2008).
[50] J. H. Rose and H. B. Shore, Phys. Rev. B **48**, 18254 (1993).
[51] M. S. Sodha and P. K. Dubey, J. Phys. D **3**, 139 (1970).
[52] R. Nyholm, A. Berndtsson, and N. Martensson, J. Phys. C **13**, L1091 (1980).